Max-Planck-Institut
für Meteorologie

REPORT No. 67

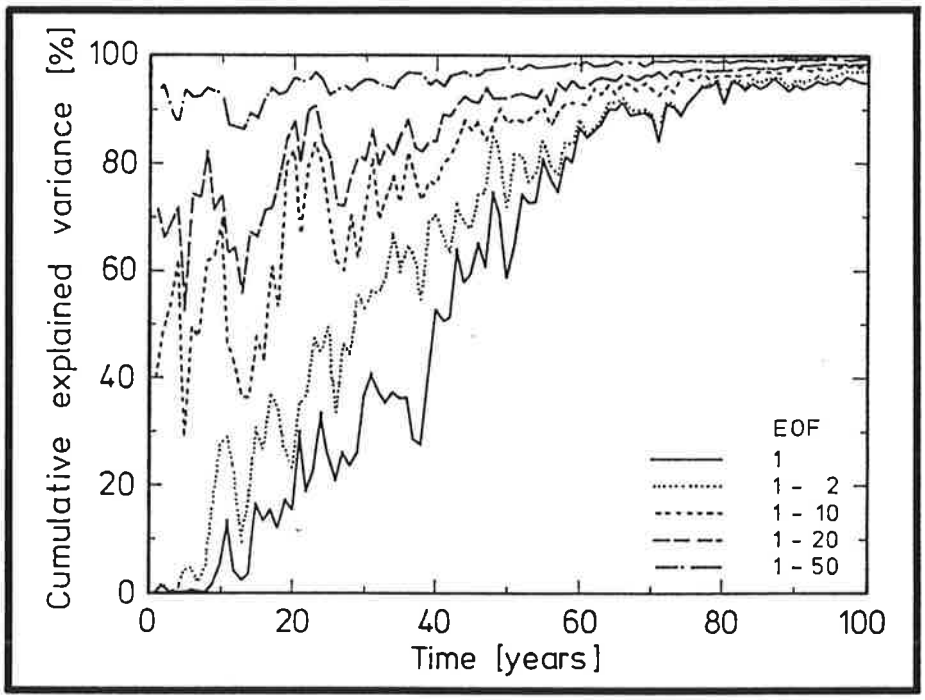

TIME-DEPENDENT GREENHOUSE WARMING COMPUTATIONS WITH A COUPLED OCEAN-ATMOSPHERE MODEL

by

ULRICH CUBASCH • KLAUS HASSELMANN • HEINKE HÖCK
ERNST MAIER-REIMER • UWE MIKOLAJEWICZ
BENJAMIN D. SANTER • ROBERT SAUSEN

HAMBURG, JULY 1991

AUTHORS:

ULRICH CUBASCH

KLAUS HASSELMANN

HEINKE HÖCK

ERNST MAIER-REIMER

UWE MIKOLAJEWICZ

BENJAMIN D. SANTER

MAX-PLANCK-INSTITUT
FUER METEOROLOGIE

ROBERT SAUSEN

METEOROLOGISCHES INSTITUT
DER UNIVERSITAET HAMBURG
BUNDESSTRASSE 55
2000 HAMBURG 13
FRG

MAX-PLANCK-INSTITUT
FUER METEOROLOGIE
BUNDESSTRASSE 55
D-2000 HAMBURG 13
F.R. GERMANY

Tel.: (040) 4 11 73-0
Telex: 211092 mpime d
Telemail: MPI.METEOROLOGY
Telefax: (040) 4 11 73-298

REPb67

Time-Dependent Greenhouse Warming Computations with a Coupled Ocean-Atmosphere Model

Ulrich Cubasch[1], Klaus Hasselmann[1], Heinke Höck[1], Ernst Maier-Reimer[1], Uwe Mikolajewicz[1], Benjamin D. Santer[1] and Robert Sausen[2]

[1] Max-Planck-Institut für Meteorologie, Bundesstrasse 55, 2 Hamburg 13, FRG

[2] Meteorologisches Institut der Universität Hamburg, Bundesstrasse 55, 2 Hamburg 13, FRG

Abstract

Climate changes during the next 100 years caused by anthropogenic emissions of greenhouse gases have been simulated for the Intergovernmental Panel on Climate Change Scenarios A ("Business as Usual") and D ("Accelerated policies") using a coupled ocean-atmosphere model. In the global average, the near-surface temperature rises by 2.6 K in Scenario A and by 0.6 K in Scenario D. The global patterns of climate change for both IPCC scenarios and for a third step-function "2xCO_2" experiment were found to be very similar. The initial warming and sea level rise due to the thermal expansion of the ocean are slower than estimated previously from box-diffusion models.

ISSN 0937–1060

1 Introduction

Detailed numerical simulations to predict the climate change caused by increasing greenhouse gases have largely been performed in the past with atmospheric general circulation models (AGCMs) coupled to a simple mixed-layer ocean with a depth of typically 50 m [1, 2, 3, 4] or to a model which parameterizes heat transport below the mixed-layer as a diffusive process [5]. A shortcoming of models of this kind is that they are unable to simulate the impact of a climate change on the ocean circulation, in particular on the oceanic heat transport and on the storage of heat in the deep ocean. These processes have a strong influence both on the equilibrium climate and on the transient climate response to external forcing. It is therefore generally recognized that reliable greenhouse warming predictions can be achieved only with simulations using fully coupled atmosphere-ocean general circulation models [6].

Two such experiments have recently been carried out [7, 8]. Although the order of magnitude of the global warming predicted by atmosphere-mixed-layer models is confirmed in these experiments, the transient response patterns differ significantly from previous predictions.

The present paper considers three further time-dependent greenhouse warming simulations together with a reference control experiment using one of the Hamburg coupled global atmosphere-ocean general circulation models. The main motivation for this study is the recent report [6] of Working Group 1 of the Intergovernmental Panel on Climate Change (IPCC), which discusses four greenhouse gas scenarios ranging from the "Business as Usual" Scenario A, in which emissions are allowed to increase unrestricted, through a set of successively more stringent abatement policies to the severest emission reduction Scenario D (Figure 1a). The IPCC scenarios are intended to provide the scientific basis for future international negotiations on the development of viable global climate policies which may have far-reaching economic implications. Since coupled ocean-atmosphere model simulations could not be carried out within the time frame of the IPCC study, however, the published IPCC scenarios had to be based on highly simplified box-diffusion models [9]. In the present study we present some results using a more realistic coupled ocean-atmosphere model for the two limiting scenarios A and D.

In addition, we have computed the transient response of the coupled system to a sudden doubling of the atmospheric CO_2 concentration. This provides a comparison with equilibrium response computations for doubled CO_2 levels performed previously with atmosphere-mixed-layer ocean models. The experiment also defines the impulse response characteristics of the

coupled system, which is useful for general theoretical transient response studies.

2 The Coupled Model

The atmospheric and oceanic components of the coupled model have been tested and applied in a variety of climate experiments [10], such as the ocean response to stochastic forcing [11], paleoclimatic studies [12, 13], and the atmospheric response to changes in radiative forcing [14]. In the coupled mode, the models were applied in a recent investigation [15] of the climatic impact of burning oil wells in Kuwait.

The atmosphere component (ECHAM) consists of a low resolution version of the spectral numerical weather forecasting model of the European Centre for Medium Range Weather Forecasts which has been modified extensively in Hamburg for climate applications. The prognostic variables are vorticity and divergence, temperature, surface pressure, water vapour and cloud water (droplets and crystals). The introduction of cloud water as an additional prognostic variable enables a more realistic simulation of clouds, precipitation and radiation [16]. The diurnal cycle is included. Sub-grid scale physical processes such as radiation, cloud formation, precipitation, convection and turbulent mixing are parameterized. The runoff into the ocean is calculated using a simple surface hydrology model.

In the current study, the horizontal resolution is limited by a triangular spectral cut-off at total wave number 21. The spectral representation is transformed to a 5.6° Gaussian grid to calculate the non-linear advection terms and physical processes. Vertically, the model is discretized on 19 levels in a hybrid σ-p-system. The semi-implicit integration scheme uses a time step of 40 minutes.

The ocean component (LSG) is based on a numerical formulation of the primitive equations [17] appropriate for large scale geostrophic motion. The nonlinear advection of momentum is neglected and fast gravity waves are strongly damped by an implicit time integration scheme using a time step of 30 days. The salinity and temperature transport through currents is computed with an upstream advection scheme. A small explicit horizontal diffusion of 200 m^2/s is introduced to counteract the inherent tendency for mode-splitting in the E-grid used in the horizontal discretization scheme. Vertical convective mixing is applied whenever the stratification becomes unstable (mainly in high latitudes, where strong surface cooling occurs). Sea ice

is computed from the ice heat balance and the advection by oceanic currents, using a simplified viscous rheology [11]. A realistic bottom topography is included.

In the present simulations, the discretization of the ocean model is based on 11 variably spaced vertical levels and two overlapping 5.6° x 5.6° horizontal grids (corresponding to an effective net grid-size of 4°) which are interpolated onto the resolution of the Gaussian grid used in ECHAM. In the coupled model simulations, the basic time step of 30 days is reduced to 1 day for the computation of sea ice and the temperature and salinity in the two uppermost ocean levels in order to resolve the more rapid response of the upper ocean to the short-term variability of the atmosphere.

The atmosphere and ocean components are coupled by the air-sea fluxes of momentum, sensible and latent heat, short and long wave radiation and fresh water (evaporation minus precipitation, plus runoff along the coastal boundaries). The fluxes are calculated in ECHAM, using as surface boundary conditions the sea surface temperature and sea ice thickness (from which the sea ice skin temperature is computed).

To avoid a climate drift of the coupled system, a flux correction is applied [18]. This is equivalent to coupling the atmosphere and ocean in anomaly response experiments by the anomalies of the fluxes computed relative to the equilibrium states of the uncoupled sub-systems. The flux correction has no impact on the computed response for small perturbations about the mean state of the model climate, provided the individual sub-systems reproduce the mean climate reasonably well.

Both models are integrated synchronously, but with their different time steps. Thus the fluxes computed at each 40 minute time step of the atmospheric model are summed over one full time step of the ocean model (1 day for the upper layers, including sea ice) and are then transferred to the uppermost layer of the ocean model.

3 Greenhouse Warming Simulations

All simulations were carried out over a 100 year period, from 1985 to 2084. In addition to the three greenhouse warming experiments (IPCC Scenarios A, D and "2xCO_2"), a control run with constant 1985 atmospheric CO_2 concentration was carried out as a reference.

The control run simulates the general structure of the mean atmospheric circulation reasonably well, although exhibiting shortcomings typical of low resolution atmospheric models which are unable to adequately resolve mid-latitude baroclinic disturbances (underestimated cyclonic activity). In the ocean, the control run reproduces the observed salinity and temperature fields and is generally consistent with the conveyor belt picture [19] of the global ocean circulation. For example, the computed 20 Sv outflow of North Atlantic deep water into the Southern Ocean and the North Atlantic heat transport of 0.6 x 10^{15} W at 30°N, two critical circulation indices, are in good agreement with independent estimates from observations [20, 21, 22, 23].

A particularly sensitive component of the coupled model is the sea ice. The flux correction is only partially effective in the ocean-ice transition zone, so that the control run required about 40 years for the sea ice distribution to equilibrate. During this initial period the annual cycle is exaggerated in the Arctic, with almost ice-free conditions in summer and refreezing in winter. Subsequently the seasonal distribution of sea ice in the control run appears reasonably realistic.

The control run is quasi-stationary with respect to the global mean near surface temperature, drifting by less than 0.4 K during the 100-year integration. The spatial temperature distribution, however, shows some drift, with high-latitude cooling in the north and warming in the south: the r.m.s. of the area-weighted temperature anomaly for the final decade of the control run (relative to the control run initial state) is 1.1°C. Since the coupled ocean-atmosphere model, like the real climate system, can be expected to exhibit natural fluctuations on time scales of a century and longer [11], it is difficult to determine whether the observed high-latitude non-stationarity of the control run represents the real natural variability of the coupled system or a spurious residual drift due to incomplete drift compensation by the flux correction. To resolve this question unambiguously, significantly longer integrations are needed than were possible for this study.

The changes occurring in the present 100-year control run are nevertheless consistent with the low-frequency variability found in a several thousand year integration of the LSG ocean model, in which the ocean was forced by short-term surface flux variations characteristic of natural atmospheric weather variability [11]. The simulated ocean circulation exhibited a pronounced red-noise variability typical of observed climate variations, the variance spectra of the oceanic heat transport and other characteristic circulation indices increasing monotonically towards low frequencies for time scales up to several centuries. We shall accordingly interpret the non-stationarity of the control run in the first instance as inherent internal variability of the

coupled model. Assuming that the natural variability arising in the control run and the response simulations are uncorrelated, we define the time-dependent climate response in the greenhouse warming simulations as the deviation with respect to the smoothed initial state of the system, as given by the average of the first ten years of the control run (Definition 1). However, we shall consider also the alternative possibility that the control run changes represent a spurious drift or a component of the natural variability which is common to all simulations. In this case it is more appropriate to define the climate response as the instantaneous difference between the greenhouse simulation and the control run at the same time instance (Definition 2).

Figure 1 shows the evolution of the atmospheric CO_2 concentrations (panel a) and the computed transient global mean temperature increase (panel b), in accordance with our Definition 1, for the three greenhouse warming simulations. Following IPCC [6], the CO_2 concentrations represent equivalent CO_2 concentrations: the net radiative forcing of all greenhouse gases is expressed in terms of an approximately equivalent atmospheric CO_2 concentration. Our "2xCO_2" value of 720 ppm equivalent CO_2 represents a doubling of the equivalent CO_2 concentration relative to the level of the early seventies, rather than 1985. The precise definition of "2xCO_2" is immaterial for our purposes, as the experiment is carried out primarily to determine the step-function response of the coupled system.

The response of the "2xCO_2" experiment shows a characteristic two-time-scale structure (see also [24]). An initial rapid temperature increase by approximately 1 K within 5 years is followed by a more gradual linear increase to a net increase of about 1.7 K after 100 years, with no sign of saturation. This is consistent with the separate time scales of the upper ocean (time scales of a few months for the mixed-layer to about a decade for the main thermocline) and the abyssal ocean (time scales of several hundred to a thousand years).

In Scenario A the temperature increases by only 0.5 K during the first 40 years, but the curve then steepens to a growth rate of ca. 0.35 K per decade to reach 2.6 K after 100 years. The temperature increase after 100 years integration for Scenario D is less than 0.6 K. The results for the latter stages of these two integrations lie between the IPCC "best" and "low estimates" [6] based on a simple box-diffusion model (Definition 2, in which the instantaneous control run is subtracted from the greenhouse simulations, is seen to yield close agreement with the IPCC "best estimates" after 100 years). However, the temperature increase during the first 50 years is consistently lower for both Scenarios A and D than for the corresponding IPCC values (independent of the response definition). This clearly has important implications

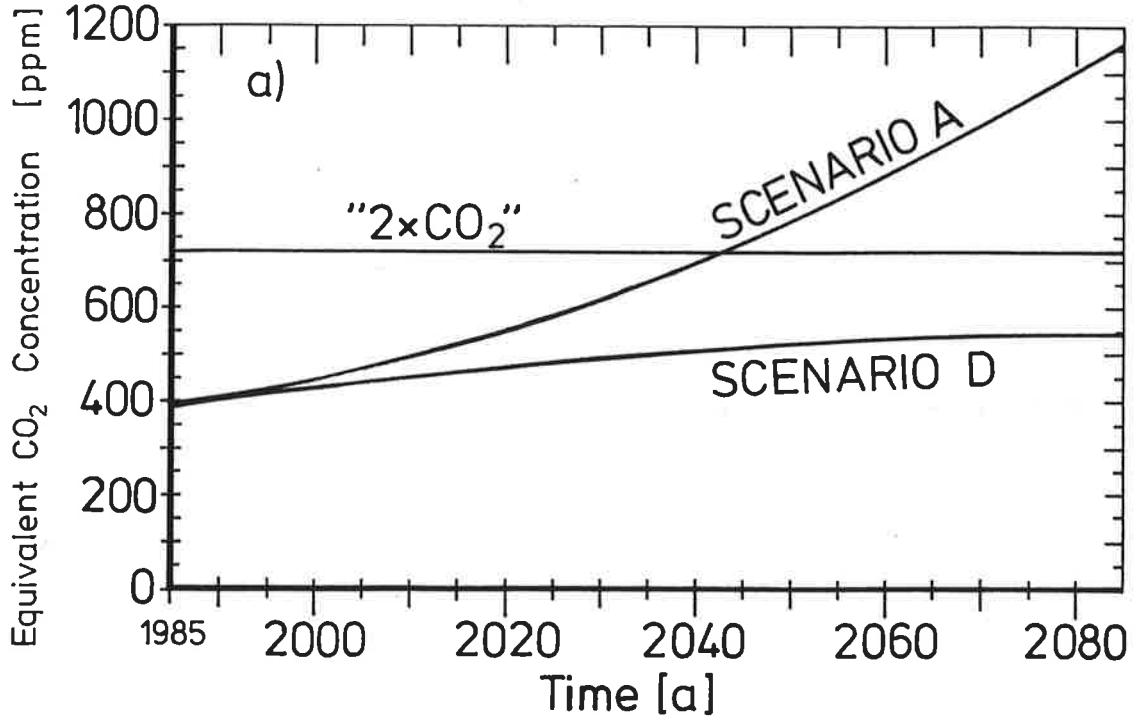

Figure 1a: Time evolution of the equivalent CO_2 concentration in the IPCC scenarios A and D and the "2xCO_2" experiment.

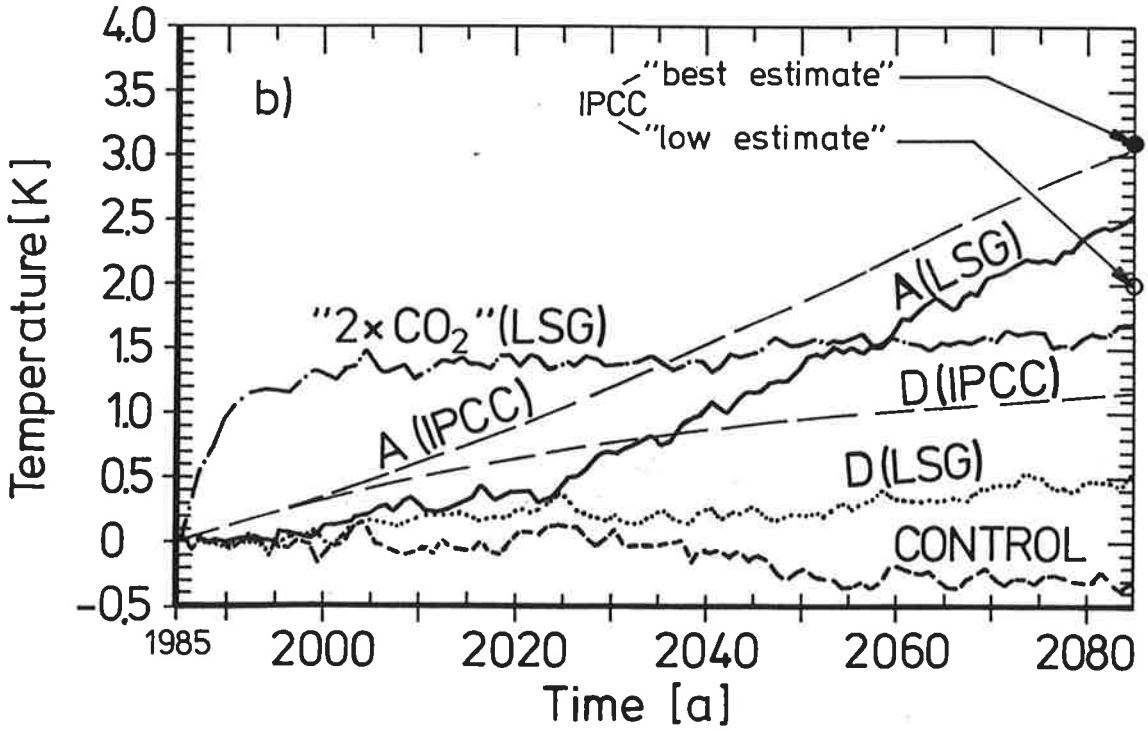

Figure 1b: Time evolution of the global mean near surface temperature change for the three greenhouse warming simulations, the control experiment and the IPCC "best estimates".

for the socio-economic impact of greenhouse warming in the early 21st century and for the greenhouse signal detection problem. However, despite the occurrence of a pronounced warming delay for both response definitions, it cannot be ruled out that this feature is an artefact of the model's natural variability [11]. Additional simulations with modified initial states and further experiments with other coupled ocean-atmosphere models are needed to establish whether this is indeed a stable feature of the real climate system. It is of interest that a similar ocean-atmosphere simulation by the Princeton group [25] exhibited an approximately linear increase without an initial depression, while another coupled model simulation using ECHAM and an isopycnal ocean model [26] yielded the same depression.

An alternative conceivable explanation of the delayed warming is the lack of a warm-up in our simulations for the period prior to 1985: the experiment was started in 1985 from an initial equilibrium state rather than from an already warming state. However, an analytical estimate based on the impulse-response characteristics of the coupled system inferred from the "2xCO_2" experiment yielded only a very small "cold start" temperature correction of less than 0.1 K.

3.1 Evolution of Surface Temperature Distributions

Figure 2a shows the global distribution of the decadal mean near surface temperature change (according to Definition 1) for the last decade of the integration (years 2076-2084) for Scenario A. The warming over the oceans is strongly reduced relative to the continents; some ocean areas (e.g. the Weddell Sea) even show a cooling. Compared with earlier atmosphere-mixed-layer model simulations, the land-sea contrast and the attenuation of the response in the Southern Hemisphere is more pronounced, indicating an enhanced heat uptake by the oceans below the mixed-layer. The largest temperature increases (up to ca. 12 K) occur where the sea ice retreats, particularly in the Arctic. The spatial patterns of the temperature change for Scenario D and the "2xCO_2" experiment (not shown) are very similar, but of smaller amplitude.

To gain more insight into the space-time structure of the transient temperature response, an eigenvector (empirical orthogonal function: EOF) analysis was carried out. The EOFs were formed using area-weighted spatial averages, without subtraction of the time means (since we were interested in the full signals), and were normalized to define an orthonormal basis.

More than 87.2% of the (time and space averaged) mean square signal for Scenario A can be explained by only two patterns (Figures 2b and 2c). The first EOF (Figure 2b) already

a Change in annually-averaged near surface temperature for the final decade of the Scenario A integration relative to the smoothed initial state of the control run

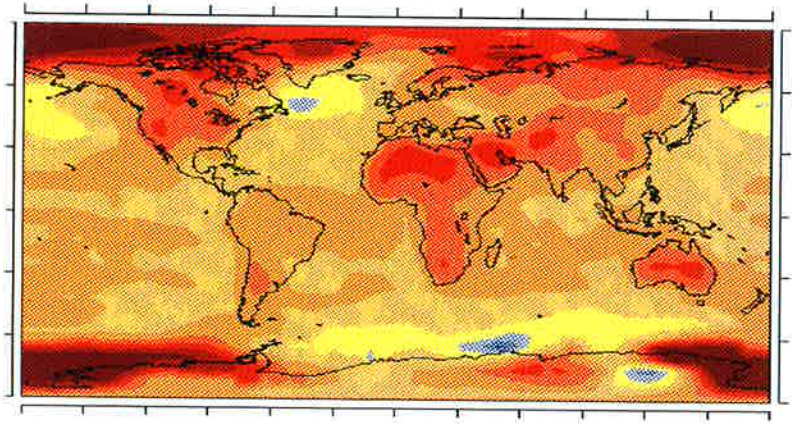

b EOF 1 of the annually-averaged near surface temperature changes for Scenario A. The explained variance is 84.1%

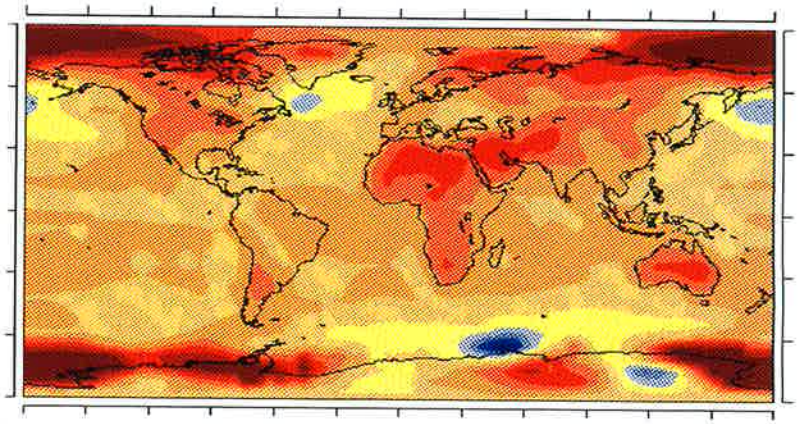

c EOF 2 of the annually-averaged near surface temperature changes for Scenario A. The explained variance is 3.1%

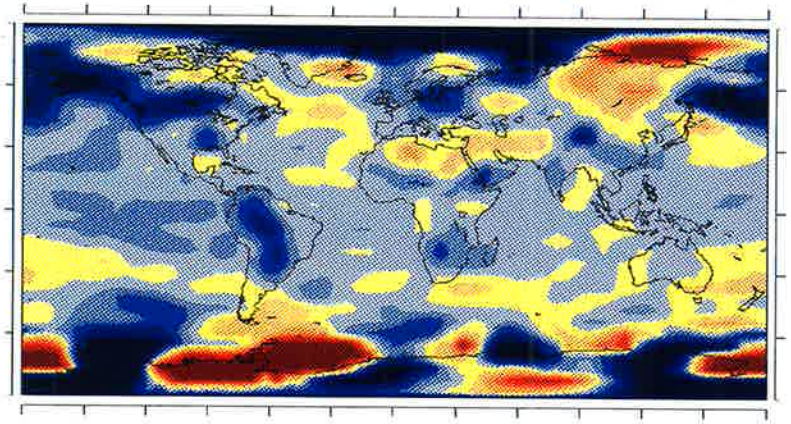

d EOF 1 of the annually-averaged near surface temperature changes for the control run. The explained variance is 52.5%

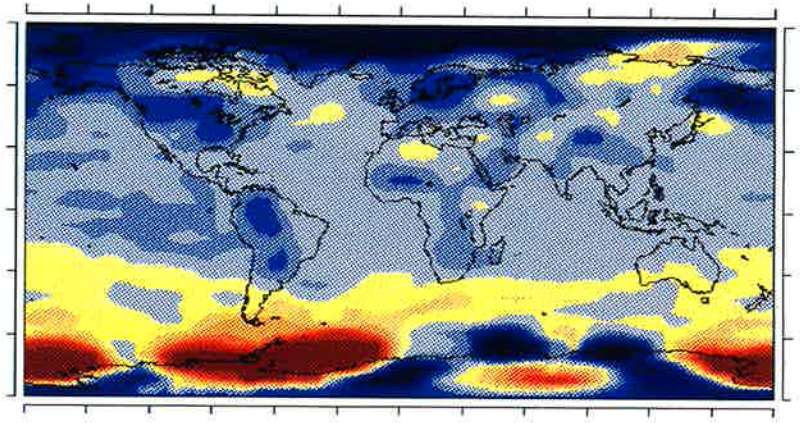

explains 84.1% of the variance, and contributes over 95% of the spatial variance of the signal in the last decade of the experiment (note the close similarity between Figures 2a and 2b).

The first two EOFs of the other simulations also explain most of the variance: 59.2% for Scenario D, 90.5% for the CO_2 doubling experiment and 71.2% for the control run. The first EOF patterns in all three greenhouse warming experiments are very similar, with pattern correlations of 0.62 for A vs D and 0.97 for A vs "2xCO_2" (the two strongest warming experiments). In contrast, the first EOF of the control run (52.5% explained variance; Figure 2d) has only a weak resemblance to these patterns: the correlation with EOF 1 of Scenario A is only 0.43. (This is associated mainly with the strong variability at high southern latitudes). Thus the dominant greenhouse warming pattern of the three response experiments cannot have been strongly affected, in the space-time average, by a possible common spurious drift or natural variability signal. However, EOF 2 of Scenario A, although contributing only 3.1% to the variance, is rather similar to EOF 1 of the control run (pattern correlation = 0.74; cf. Figures 2c,2d). Thus this component of the greenhouse warming signal could contain a spurious drift or natural variability contribution. This is supported by the strong variability exhibited by this pattern in the vicinity of the Antarctic Circumpolar Current, a relatively unstable region of the ocean circulation in which a similar variability was found also in the above-mentioned stochastically forced ocean experiment [11]. However, it should be pointed out that for physical reasons the patterns of natural variability and the response of the system often tend to be similar, so that a high pattern correlation in itself is not necessarily evidence of a contamination of the greenhouse warming signal by natural variability noise [27].

The relation between the greenhouse signal and the natural variability or drift of the coupled model becomes clearer if the evolution of the patterns with time is considered. Figure 3 shows the evolution of the cumulative EOF contributions to the explained spatial variance for Scenario A. The contribution from the first EOF is seen to grow monotonically, completely dominating the greenhouse warming pattern towards the end of the integration. There is little doubt that the first EOF represents a real signal, since, as pointed out above, essentially the same pattern is found in all three greenhouse experiments and the pattern is not strongly correlated with the dominant variability pattern of the control run.

In the first half of the Scenario A experiment, the response is composed of many EOF patterns. The contribution from the second EOF in this period is comparable to that of EOF 1, and both patterns initially represent only a small fraction of the total spatial variance. The

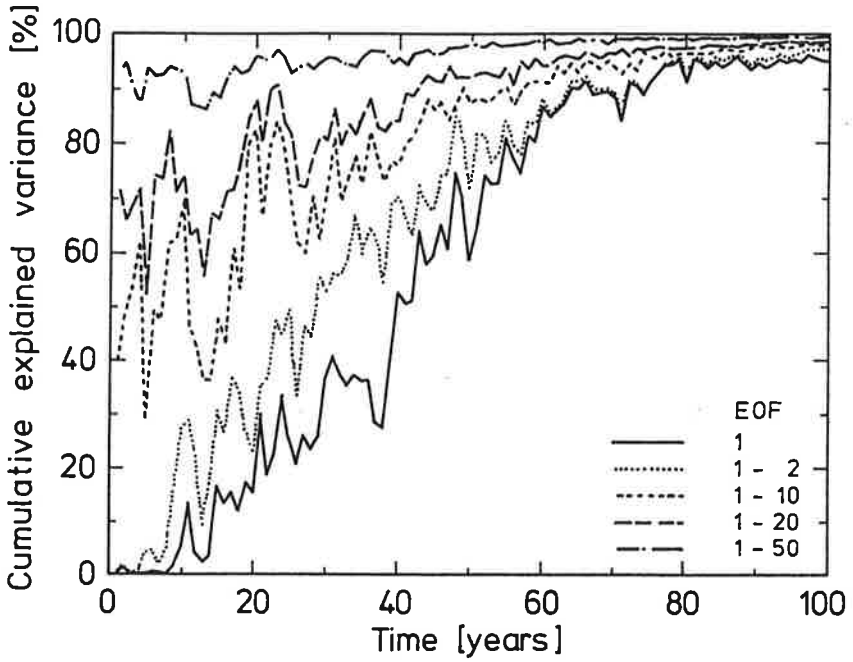

Figure 3a: Cumulative explained spatial variance as a function of time and number of EOFs (1, 2, 10, 20 and 50) for Scenario A. The signal is defined as the difference relative to the smoothed initial state (average over years 1-10) of the control run. Results are for annually averaged 2 m temperature.

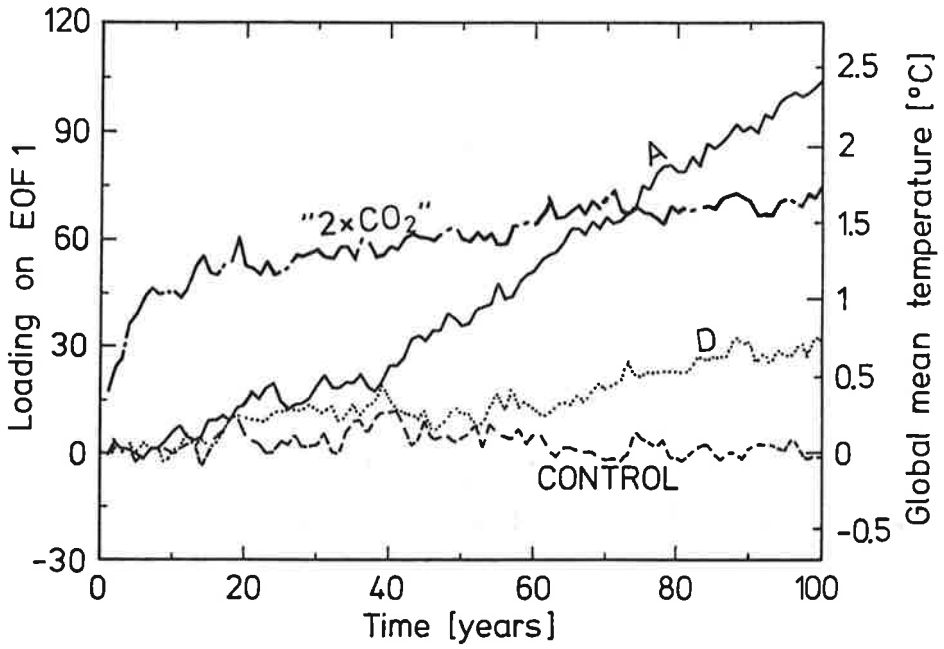

Figure 3b: Principal component time series for the projection of the temperature response fields of the three greenhouse warming experiments and the control run onto EOF 1 of Scenario A. The ordinate axis on the right hand side of the figure indicates the contribution of EOF 1 to the global mean temperature (cf. Figure 1b).

relative contribution from EOF 2 is largest in the fourth decade, during the transition from the slow to the more rapid temperature response regime (cf. Figure 1b). Since, as just discussed, the EOF 2 pattern is the one which is most prone to contamination by natural variability, we repeated the analysis using Definition 2 for the greenhouse response (subtraction of the instantaneous rather than the initial control run state from the greenhouse simulation). This did not reduce the EOF 2 contribution: the cumulative variance curves were found to be similar to those of Figure 3, with an even stronger EOF 2 signal in decades 3-5.

To intercompare the temporal evolution of the spatial response patterns of the three greenhouse simulations and the control run on a common basis, the signals (according to Definition 1) of all experiments were projected onto the EOFs of Scenario A. The coefficient (principal component) time curves for the projection on EOF 1 (Figure 3b) support our previous conclusion that most of the signal can be explained by the same pattern in all three greenhouse experiments, while the coefficient of this pattern for the control run is small. The similarity of the curves in Figures 1b and 3b is explained by the fact that the first EOF largely determines the global mean temperature (the spatial mean of EOF 1 is almost five times larger than that of EOF 2; the contribution of EOF 1 to the global mean temperature is indicated by the ordinate axis on the right hand side of Figure 3b).

3.2 Temperature Sections

Vertical sections of the temperature anomaly distribution (according to Definition 1) established in the last decade of the integration for Scenario A are shown in Figures 4a (atmosphere) and 4b,4c (ocean). The warming in the atmosphere is largest in the tropical tropopause (Figure 4a), while the stratosphere shows, as expected, an extensive cooling. The maximum warming of the oceans takes place in the uppermost levels, with a maximum of more than 2 K in the tropical regions. The warming penetrates into the deep ocean in the high latitude regions of deep convection, mainly the Northern Atlantic, the Weddell Sea and the Ross Sea (Figures 4b,c). These regions generally coincide with the regions of low warming or even cooling at the surface (Figure 2a, cf. also [8]).

The stabilization of the water column through surface warming tends to suppress deep convection. This inhibits the mean heat uptake from the deep ocean in high latitudes, further counteracting the surface ocean greenhouse warming in these regions. In Scenario A, the global

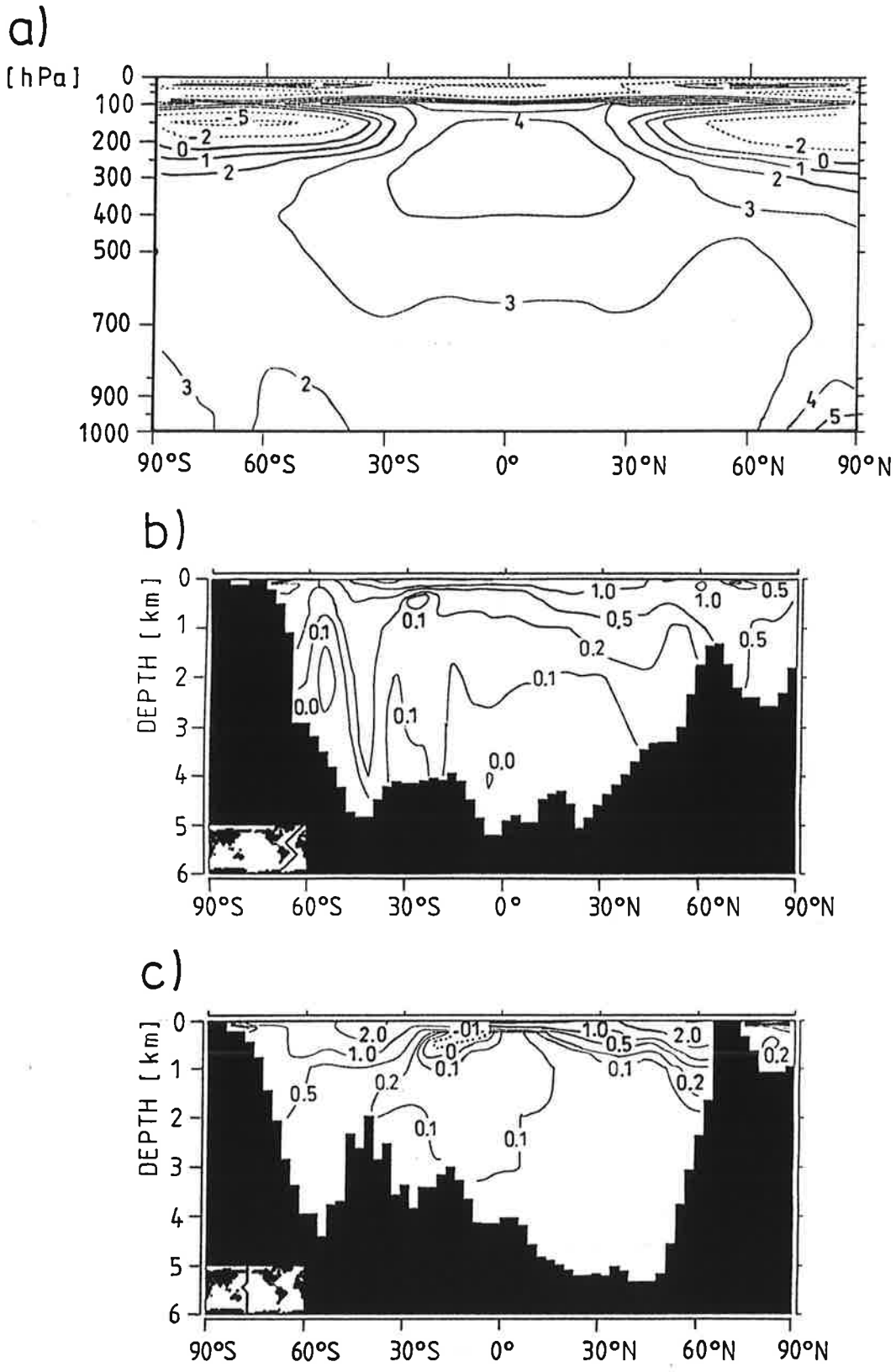

Figure 4: Vertical cross-section of zonally averaged changes in atmospheric temperature (**a**) and vertical cross-section of temperature changes in the Atlantic (**b**) and Pacific (**c**) along the GEOSECS transect. Results are for the final decade (years 2076-2084) of Scenario A relative to the smoothed initial state (average over years 1-10) of the control run.

deep water formation is reduced by about 30% at the end of the experiment, with a corresponding retardation of the thermohaline circulation. The resulting longer surface exposure time produces a positive surface salinity anomaly in regions of high evaporation in the subtropical gyres and a negative surface salinity anomaly in high latitude precipitation regions, for example in the North Atlantic [28]. The reduction in the global overturning of the ocean also reduces the uptake rate of CO_2 in the ocean [17], producing a positive greenhouse warming feedback.

3.3 Evolution of Sea Level

An important consequence of global warming is the sea level rise due to the melting of glaciers, changes in other components of the hydrological cycle, and the thermal expansion of the ocean. The first effect is not included in our model. The second effect is very small, of the order of 1 or 2 cm. The third contribution is also relatively modest in our 100 year simulations. The global mean sea level rise after 100 years due to thermal expansion is computed as 15 cm for Scenario A, 5 cm for Scenario D and 16 cm for the "2xCO_2" experiment (Figure 5).

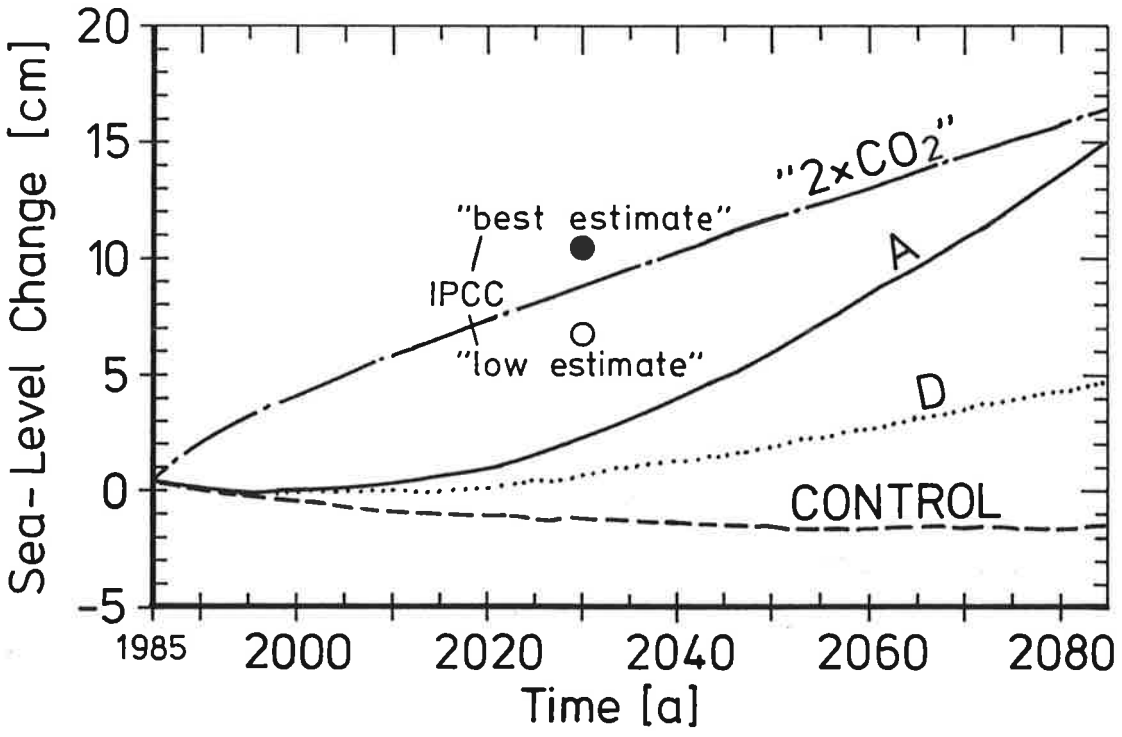

Figure 5: Time evolution of global mean sea level changes (due to thermal expansion of the ocean) in the two IPCC scenarios, the "2xCO_2" experiment and the control run. The IPCC estimates for Scenario A (thermal expansion effects only) in 2030 are marked.

Regionally, non-uniform warming and dynamical effects yield variations in sea level rise of the same order as the global mean [28]. The predicted mean sea level rise due to thermal expansion is approximately half that of the IPCC projections [6]. This reflects the slower temperature response in the first half of our Scenario A and D experiments relative to the corresponding IPCC estimates (see Figure 1b; the "cold start" depression in sea level was estimated as less than 2 cm).

Published estimates of the equilibrium global sea level rise due to the thermal expansion of the oceans for the equilibrium climate response to a CO_2 doubling generally lie in the range of 50 cm. Our significantly lower predictions for the transient sea level response within one century are not inconsistent with these predictions and are supported by the time dependent sea level computation in a 2000 year integration made with the LSG ocean model [28]. The simulation yielded an asymptotic sea level rise of 50 cm, but the increase in sea level was found to be a very slow process requiring several hundred years adjustment time.

4 Conclusions

Simulations with a global coupled atmosphere-ocean model of the greenhouse warming over the next 100 years for the IPCC Scenarios A ("Business as Usual") and D ("Accelerated Policies") and a "2xCO_2" experiment support the order of magnitude predictions of the IPCC report [6]. However, they differ significantly with respect to the detailed transient and spatial response characteristics. The global average near-surface temperature increase of 2.6 K in Scenario A and 0.6 K in Scenario D at the end of the simulation lie close to the IPCC "best estimate", but the global average temperature changes in years 10-50 of Scenarios A and D are consistently lower than the corresponding IPCC values. This could be due to the stronger oceanic heat uptake resulting from a more realistic description of the deep ocean in the present model. However, more experiments are needed to establish whether the delayed warming is a stable feature of the real climate system. Pronounced warming occurs in the deep ocean in high latitude regions of penetrative convection, mainly in the Northern Atlantic, the Weddell Sea and the Ross Sea. These areas coincide with regions of low warming or even initial cooling at the surface, a feature which cannot be simulated by models with mixed-layer oceans.

A single common temperature response pattern establishes itself as the dominant climatic signal in the later stages of all three greenhouse experiments. It is characterized by a significantly

larger warming over land areas than over oceans, and a corresponding attenuation of the warming in the Southern Hemisphere. This pattern can be clearly distinguished from the internally-generated natural variability (or possibly residual drift) in the control run. In the first 50 years of the simulation, however, the greenhouse signal contains additional patterns of comparable magnitude which cannot be so clearly separated from the model's natural variability.

The global sea level rise due to the thermal expansion of the ocean is only 15 cm after 100 years for Scenario A, 5 cm for Scenario D and 16 cm for the CO_2 doubling experiment. These values are half as large as the corresponding IPCC estimates and are probably a consequence of the delayed temperature response in our experiments. Regional variations in sea level rise due to variations in warming and dynamical effects are of the same order as the global mean. Our small sea level rise values imply only a delay in the sea level response arising from the thermal expansion of the oceans and are not inconsistent with previous estimates [6, 9, 28] of an asymptotic equilibrium thermal sea level rise of 50 cm for a CO_2 doubling.

ACKNOWLEDGEMENTS

This work was sponsored by the Bundesministerium für Forschung und Technologie, the Commission of the European Community, the Max-Planck-Gesellschaft and the Freie and Hansestadt Hamburg. The authors would like to thank the staff of the Deutsches Klimarechenzentrum, the Meteorologisches Institut der Universität Hamburg and the Max-Planck-Institut für Meteorologie for their support, particularly A. Bierkamp, O. Böhringer, M. Böttinger, W. Brüggemann, M. Grunert, F. Lunkeit, H. Luthardt, N. Noreiks, J.M. Oberhuber, M. Ponater, E. Roeckner, U.Schlese, D. Schriever, R. Voß, W.Welke and M. Windelband.

References

[1] Washington, W.M. & Meehl, G.A. *J. Geophys. Res.* **89**, 9475-9503 (1989).

[2] Wetherald, R.T. & Manabe, S. *J. Atmos. Sci.* **45**, 1397-1415 (1988).

[3] Mitchell, J.F.B., Wilson, C.A. & Cunningham, W.M. *Quart. J. R. Meteorol. Soc.* **113**, 293-322 (1987).

[4] Schlesinger, M.E. & Mitchell, J.F.B. *Rev. of Geophys.* **25**, 760-798 (1987).

[5] Hansen, J., Fung, I., Lacis, A., Rind, D., Lebedeff, S., Ruedy, R., Russell, G. & Stone, P. *J. Geophys. Res.* **93**, 9341-9364 (1988).

[6] Houghton, J.T., Jenkins, G.J. & Ephraums, J.J. (eds.) *Climate Change. The IPCC Scientific Assessment* Cambridge University Press, 1990.

[7] Washington, W.M. & Meehl, G.A. *Climate Dyn.* **4**, 1-38 (1989).

[8] Stouffer, R.J., Manabe, S. & Bryan, K. *Nature* **342**, 660-662 (1989).

[9] Wigley, T.M.L. & Raper, S.C.B. *Nature* **330**, 127-131 (1987).

[10] Hasselmann, K. *Tellus* (in press).

[11] Mikolajewicz, U. & Maier-Reimer, E. *Climate Dyn.* **4**, 145-156 (1990).

[12] Maier-Reimer, E. & Mikolajewicz, U. *Oceanography 1988* (eds Ayala-Castanares, A., Wooster, W. & Yanez-Arancibia, A.) UNAM Press Mexico D.F., 87-100 (1989).

[13] Lautenschlager, M. & Herterich, K *J. Geophys. Res.* **95**, 22,547-22,557 (1990).

[14] Cess, R.D. et al. *Science* **245**, 513-516 (1989).

[15] Bakan, S., Chlond, A., Cubasch, U., Feichter, J., Graf, H., Graßl, H., Hasselmann, K., Kirchner, I., Latif, M., Roeckner, E., Sausen, R., Schlese, U., Schriever, D., Schult, I., Schumann, U., Sielmann, F. & Welke, W. *Nature* **351**, 367-371 (1991).

[16] Roeckner, E., Dümenil, L., Kirk, E., Lunkeit, F., Ponater, M., Rockel, B., Sausen, R. & Schlese, U. *Research Activities in Atmospheric and Oceanic Modelling*. WMO Technical Document **322**, Geneva, (1989).

[17] Maier-Reimer, E. & Hasselmann, K. *Climate Dyn.* **2**, 63-90 (1987).

[18] Sausen, R., Barthel, K. & Hasselmann, K. *Climate Dyn.* **2**, 154-163 (1988).

[19] Broecker, W.S., Andree, M., Wolfli, W., Oeschger, H., Bonani, G., Kenett, J. & Peteet, D. *Paleoceanography* **3**, 1-19 (1988).

[20] Hall, M.M. & Bryden, H.L. *Deep-Sea Res.* **29A**, 339-359 (1982).

[21] Hsiung, J. *J. Phys. Oceanogr.* **15**, 1405-1413 (1985).

[22] Gordon, A.L. & Piola, A.R. *J. Phys. Oceanogr.* **13**, 1293-1300 (1983).

[23] Roemmich, D. *J. Phys. Oceanogr.* **10**, 1972-1983 (1980).

[24] Manabe, S., Bryan, K. & Spelman, M.J. *J. Phys. Oceanogr.* **20**, 722-749 (1990).

[25] Manabe, S., personal communication, cited in Chapter 6 of *Climate Change. The IPCC Scientific Assessment* Houghton, J.T., Jenkins, G.J. & Ephraums, J.J. (eds.) Cambridge University Press, 1990.

[26] Lunkeit, F. & Oberhuber, J.M. personal communication (1991).

[27] Liu, Q. & Schuurmanns, C.J.E. *Geophys. Res. Lett.* **17**, 1085-1088 (1990).

[28] Mikolajewicz, U., Santer, B.D. & Maier-Reimer, E. *Nature* **345**, 589-593 (1990).